Numerical study of geometrical frustration in a planar soft-hard magnetic system

Hemachander Subramanian and J. E. Han
Department of Physics, State University of New York at Buffalo, Buffalo, New York 14260, USA
(Received 5 May 2008; revised manuscript received 17 September 2008; published 14 October 2008)

We computationally study the frustrated macroscopic magnetic configurations of a thin soft-magnetic layer on top of a hard magnet geometrically patterned as three equidistant disks. The interplay between competing exchange, magnetostatic, and Zeeman interactions, enhanced by the geometric constraints, results in rich magnetization configurations when an external magnetic field is rotated around the sample. We identify four successive ranges of the external field magnitude in each of which the system exhibits unique energetics and chooses different sets of energy minima during the rotation of the external magnetic field. The system can be used as a ternary logic storage device, with read and write operations achieved by utilizing the unique behavior of the system in each of the four regimes.

DOI: 10.1103/PhysRevB.78.134410 PACS number(s): 71.70.Gm, 75.40.Mg, 85.70.Ay

INTRODUCTION

Magnetic systems with artificial geometrical frustration have attracted considerable attention for the presence of multiple ground states and intricate magnetic properties.[1,2] Soft-hard magnetic structures have recently been intensively investigated for their high coercivity and saturation magnetization properties.[3–5] Exchange-coupled planar soft-hard magnetic layers[6–10] have been the model systems of study in exploring the dependency of effective exchange coupling between the hard and soft-magnetic materials on the micromagnetic parameters. These systems show a rich variety of magnetic configurations when magnetic frustration is induced geometrically. This is particularly the case when the characteristic length of magnetization configuration is comparable to the size of the device features.[11] The interaction between the macroscopic geometry of the system and the magnetic configurations exhibited by the system is more pronounced at the nanometer length scale since the exchange-correlation length of most magnetic materials falls in the nanometer range.

Previous works on soft-hard magnetic systems[12–15] have mostly focused on magnetization configurations between layers of soft-hard magnets. In this paper, we study two-dimensional geometry-induced multiple magnetic configurations and external magnetic-field-induced transitions between these configurations. We concentrate on the magnetization configurations in the plane of the soft magnet, determined by the magnetization directions of the constraining hard magnets and an external field.

The combined effect of changing energy landscape due to external field magnitude variation and the multiple energy minima arising out of geometric frustration results in the system exhibiting distinct behaviors at different external field strengths. We identify four distinct regimes of behavior of the system, parametrized by the magnitude of the external field. By changing the external field magnitude, the system can be switched between these regimes. In contrast, by rotating an external magnetic field of constant magnitude and thereby staying within a regime, the system can be made to switch between the originally degenerate energy minima due to geometrical frustration (see Fig. 1). The goals of this paper are to study the interaction of the effects of variation in direction and magnitude of the external field on the magnetization of the geometrically frustrated system and to computationally demonstrate the feasibility of constructing a ternary logic device using the system, which would be useful in applications where ambiguity, irrelevant data, or error needs an additional representation.[16–18]

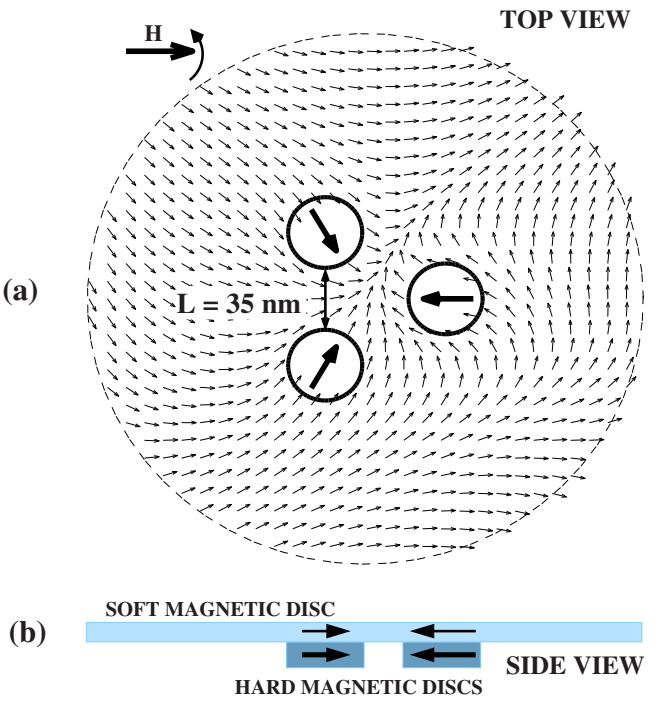

FIG. 1. (Color online) (a) Two-dimensional soft-hard magnetic composite system. The magnetic structure in the soft-magnetic region is determined by the boundary condition fixed by the hard magnetic disks and external field **H**. One of the many possible energy minima, with two magnetic influx and one outflux between the disks, is shown. The length scale of the system, L, defined as the distance between the two hard magnetic disks, is shown. (b) Side view of the device.

SYSTEM DESCRIPTION

The two-dimensional soft-hard magnetic system under study consists of three hard magnetic disks placed underneath a thin soft-magnetic layer (see Fig. 1). The three hard magnets, placed on vertices of an equilateral triangle, are chosen to have their magnetizations pointing toward the center of the triangle. The roles of the hard magnets are to fix the direction of magnetization of the soft magnet as the same as that of the underlying hard magnet at the interface and to introduce frustration in the system. We assume that the magnetization of the soft-magnetic layer is in plane and that the soft-magnetic layer is thin enough (5 nm) that its magnetization direction varies little across the width of the layer. This assumption is justified by experiments which show that the strong exchange coupling between the hard and soft-magnetic layers results in a single-domain-like behavior of the bilayer for the geometrical parameters and the external magnetic-field range relevant for this study.[6] Figure 1 shows one of the possible energy minimum configurations of the soft-hard magnetic system. This and the following figures show coarsely sampled magnetization vectors from denser data for better visual clarity.

The experimental realization of the system described above, though challenging with current state-of-the-art technologies, is possible in the very near future with the improvements in electron-beam lithographic, deep UV interference, and self-assembly techniques, propelled by the demand from the high-density magnetic memory market. As an example of the advancement of lithographic techniques, Cowburn *et al.*[19] demonstrated fabrication of single-domain circular nanomagnets of 6 nm thickness and 55 nm diameter, which is close to the size of the hard disks used in the system described above. Assembling the three hard magnetic disks with their crystallographic easy axes pointed as shown in Fig. 1(a) requires technologies that are still in the nascent stage. We believe that it can be achieved in near future.[20–26] A preliminary analysis indicates that the system's behavior is nearly the same when the hard magnetic disks are replaced by hard magnetic rods at appropriate positions. The shape anisotropy of the rods makes it easier to pin the direction of the magnetization of the rods along the directions required in our system.

MODEL

The Hamiltonian density of the system is

$$\mathcal{H} = A|\nabla \mathbf{m}|^2 - \frac{1}{2}M_0^2 \mathbf{m}\cdot\mathbf{h}' - M_0^2 \mathbf{m}\cdot\mathbf{h} + V_0 M_0^2 (|\mathbf{m}|^2 - 1)^2 \tag{1}$$

in cgs units. Here, $\mathbf{m}$ is the magnetization vector normalized to the saturation magnetization M_0, A is the exchange stiffness, $\mathbf{h}$ is the applied magnetic field normalized to M_0, and $\mathbf{h}'$, the dipole field normalized to M_0, is given by

$$\mathbf{h}'(\mathbf{r}) = \int d^3\mathbf{r}' \frac{3\hat{\mathbf{n}}[\hat{\mathbf{n}}\cdot\mathbf{m}(\mathbf{r}')] - \mathbf{m}(\mathbf{r}')}{|\mathbf{r}-\mathbf{r}'|^3}, \tag{2}$$

where $\hat{\mathbf{n}}$ is the unit vector along $\mathbf{r}-\mathbf{r}'$. The role of the last term in Eq. (1) is to impose the condition of $|\mathbf{m}|=1$.[11] The system is discretized as a two-dimensional rectangular mesh of magnetization vectors.

The first term in Eq. (1) is the exchange term, approximated for a continuous dipole distribution.[27] The second term is the dipole-dipole interaction term. The third term is the Zeeman energy of a dipole in an external magnetic field $\mathbf{h}$. The last term with a large value of V_0 is concocted to preserve $|\mathbf{m}|^2=1$ condition during numerical energy minimization. Inclusion of the condition $|\mathbf{m}|^2=1$ in the energy functional had better numerical behaviors than a direct imposition of the constraint. The resulting energy minima satisfied the condition $|\mathbf{m}|^2=1$ accurately.

We assign the values of bulk nickel, a typical ferromagnet, for A and M_0, $V_0=100$.[11] We let the external magnetic field, $|\mathbf{H}|=M_0|\mathbf{h}|$, of varying magnitudes rotate around the system to drive the transitions and evaluate the minimum-energy configurations for all external field directions. Typical values of radius of hard magnets, distance between hard magnetic centers, and the radius of the soft-magnetic circle are 20, 75, and 150 nm, respectively. The soft magnet is taken to be circular to preserve the threefold symmetry of the system, although the symmetry need not be exact. The magnetocrystalline anisotropy is assumed to be absent in the soft magnet and very high in the hard magnetic disks, so that the magnetizations of the disks are frozen in the direction of the least anisotropy energy.

The system was simulated on a rectangular lattice of size 128×128. For energy minimization, we used the conjugate gradient method.[28] Polak-Ribiere method was used in updating the search directions for minimization.[29] The demagnetization energy calculation was simplified by writing $\mathbf{m}\cdot\mathbf{h}'$ as $\Sigma_{i,j}\mathbf{m}_i\cdot\mathbf{D}(\mathbf{r_i}-\mathbf{r_j})\cdot\mathbf{m}_j$, where the components of the 3×3 demagnetization tensor $\mathbf{D}(\mathbf{r_i}-\mathbf{r_j})$ are given by

$$[D(\mathbf{r_i}-\mathbf{r_j})]_{\alpha\beta} = \int_{V_i} d^3\mathbf{r_i} \int_{V_j} d^3\mathbf{r_j} \frac{3\hat{n}_{i\alpha}\hat{n}_{j\beta} - \delta_{\alpha\beta}}{|\mathbf{r}_i - \mathbf{r}_j|^3}. \tag{3}$$

Here the integrations are over the volume elements V_i, V_j of uniform magnetization located at the mesh points i and j and $\hat{\mathbf{n}}_i$ and $\hat{\mathbf{n}}_j$ are the unit vectors in the direction of the uniform magnetization at the mesh points i and j. The demagnetization tensor $\mathbf{D}(\mathbf{r_i}-\mathbf{r_j})$ is independent of magnetization and is dependent only on the geometry of the system. Hence it was calculated once and the values were stored for the entire run. The calculations were done using the results in Ref. 30. The calculation time of the dipole interaction energy was reduced significantly using fast Fourier transform, using the fact that the convolution of the demagnetization tensor and the magnetization vectors transform into a direct multiplication in the Fourier space.[29] The energies of the magnetization configurations generated by our program agreed well with the energies calculated using OOMMF software,[31] which integrates Landau-Lifshitz micromagnetic equation to arrive at equilibrium configurations.

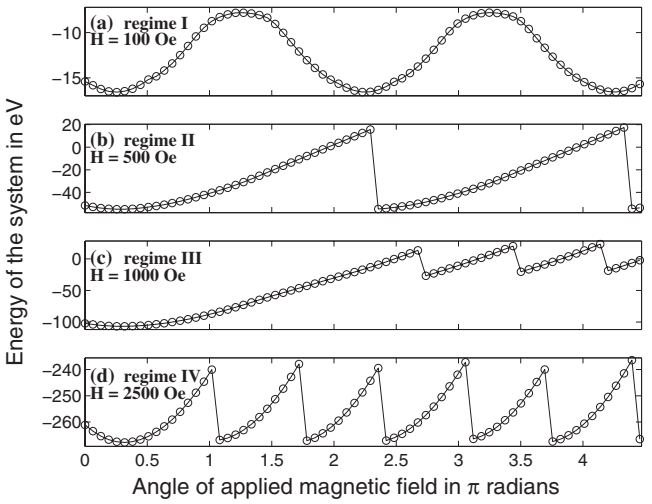

FIG. 2. Variation in energy of the system at different regimes with respect to the angle of externally applied field, starting from the initial configuration shown in Fig. 1. Plot (a) shows the variation in energy in the first regime. No transitions are seen. The external field is not strong enough to dislodge the system from the energy minimum that it stays in. (b) shows the behavior of the system in the second regime. One transition occurs in an interval of 2π radian rotation of external field. A static domain-wall shield forms and vanishes during transition. (c) shows the energy variation in third regime. The energy never drops to the initial low-energy state the system started in. The system stays in metastable states and all the transitions are between three equivalent metastable states characterized by switching of the domain-wall shield from one pair of hard disks to another. (d) shows the variation in energy in the last regime. High external field aids the system to escape from one minimum to another easily. Three transitions happen in a 2π radian rotation of external field.

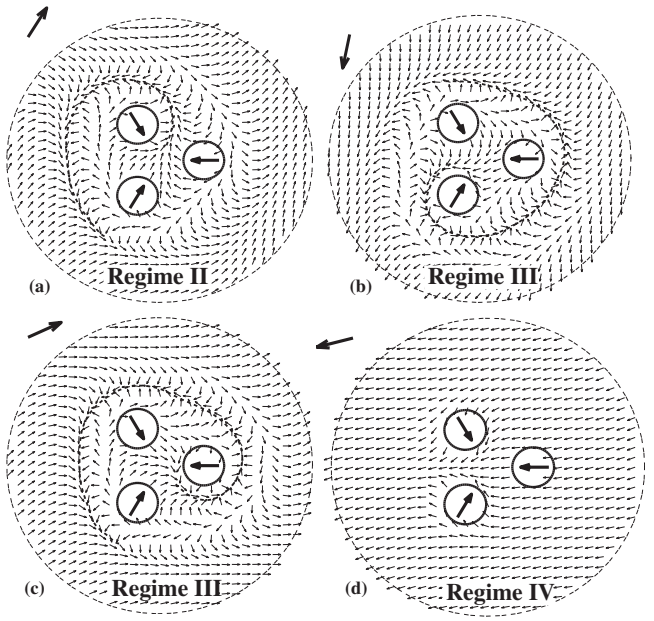

FIG. 3. Magnetization configurations of the system at different regimes. (a) shows the domain-wall formation in the second regime at an external field of 500 Oe. This domain wall does not switch to another pair of hard magnetic disks as the external field is rotated. (b) and (c) show domain-wall shields in the third regime at an external field of 1000 Oe. In this regime, the domain-wall shield switches to the next pair of hard magnetic disks as the external field is rotated. The system stays in these metastable states and never drops down to the ground state. (d) shows the system in the fourth regime at an external field of 2500 Oe. The magnetization follows the external field faithfully. The arrows to the top left of the figures show the direction of the external field. The appearance of domain-wall shield is enhanced by a dotted line to aid visualization.

SYSTEM IN AN EXTERNAL ROTATING MAGNETIC FIELD

When the magnitudes of exchange, magnetostatic, and Zeeman energies are of the same order, energy minimization leads to apportioning of the geometrically induced strain to the different energies variously. This leads to interesting magnetic configurations, which we classify as regimes. The energy landscape changes considerably across the regimes, as the external field magnitude changes, and the system accesses different local energy minima at different regimes. In the following description of the four regimes, the initial configuration of the system is chosen, among other equally good options, to be the one in which the magnetization flows through the neck between top left and the right disk when the external field angle is zero radian. This initial configuration is shown in Fig. 1.

In the first regime (I), characterized by the applied field magnitude less than approximately 150 Oe, the exchange and magnetostatic energies are stronger than the Zeeman energy due to the applied field, and the system hardly responds to the field. Figure 1(a) shows the system's magnetization configuration in one of the minimum-energy states. Figure 2(a), plotted between the angle of external magnetic field and the energy of the system in eV, shows no major transitions. The system nearly retraces its old path in the phase space when the external field is rotated in the other direction.

In the second regime (II), characterized by applied field magnitudes in the range of 150–700 Oe, we start from the initial configuration and rotate the magnetic field from zero radian, counterclockwise. The system forms a domain wall that shields the magnetization near the three disks from rotating away from the direction of that of the hard disks and separates it from the periphery where the magnetization roughly follows the external field [Fig. 3(a)]. The domain wall shields the magnetization near two disks on the left, and the magnetization escapes through the neck between top left and the right hard magnetic disks, as it did in the initial configuration, and does so for one full rotation of the external field of constant magnitude. When the external field completes one full rotation, the system makes a transition to the initial configuration, shown in Fig. 1, without the domain wall. The plot of energy (eV) versus applied field angle shown in Fig. 2(b) shows the 2π periodicity.

As the external field magnitude is increased from 700 Oe, the system enters the third regime (III) where the geometrical constraint yields to Zeeman energy and the hysteresis curve starts exhibiting the degeneracy introduced by the geometry.

Initially, the system takes approximately 2.5π radians to reach the high-energy-density configuration, following the same path as that of the second regime before switching to the typical third regime behavior. The domain-wall shield that straddled the two hard magnetic disks for the whole of 2π rotation of the external field in the previous regime now switches with the field from shielding one neck to shielding the neighboring neck and covers all three necks successively during one full rotation of external field of constant magnitude. Figures 3(b) and 3(c) show the domain-wall shield covering two different necks for two different angles of external field. Figure 2(c) shows the variation in energy (eV) with respect to the applied field angle. The system can be said to be oscillating between three metastable states which are configurationally different from the ground state depicted in Fig. 1. The system never reaches the ground state during this regime because of the lack of a monotonically decreasing energy pathway from the metastable configuration to the ground-state configuration in the presence of an external magnetic field.

From 2500 Oe onward, the Zeeman energy dominates all other energies of the system, and the system starts following the external field and is in regime (IV). As the field rotates, the magnetization switches from its initial configuration to flow through the neck in the direction of the field. There are three transitions and the system switches between three equivalent minimum-energy states. Figure 3(d) shows one of the three minimum-energy states. Figure 2(d) shows the variation in energy of the system (in eV) with respect to the angle of the applied field for a field strength of 2500 Oe. The plot exhibits a periodicity of $\frac{2\pi}{3}$ radians, and the three transitions corresponding to the switching of the system between three minimum-energy states can be seen. This plot has to be contrasted with Fig. 2(b) of the second regime, where the periodicity is 2π radians.

The transition between these four regimes is not sharp. At the intermediate external field magnitudes, the system is unstable to small external perturbations and fluctuates between the regimes on either side. Also, these rich magnetization configurations occur only in a restricted regime of geometrical parameters of the system, where the increase in energy of the system due to frustration is comparable to that of other energies of the system. Quantitatively, our regime of interest lies where the exchange length of the system is of the order of the characteristic length scale L introduced by the geometry, which in our case is the size of the neck between any two disks. The exchange length of nickel is $\sqrt{\frac{A}{M_0^2}} \approx 17$ nm, whereas L is 35 nm. When L is increased to 70 nm, the system neutralizes geometric frustration by forming domains around the hard magnets with the magnetization direction of the domains pegged along that of the hard magnets. An example of such domain formation is shown in Fig. 4. The figure shows a system in which the radius of hard magnets, distance between hard magnetic centers, radius of the soft-magnetic circle, and thickness of the sample are assigned values 40, 150, 300, and 20 nm, respectively.

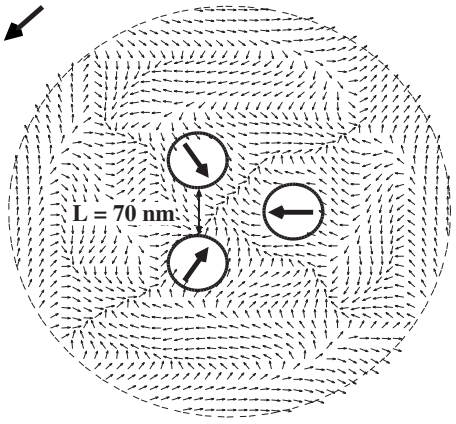

FIG. 4. Domain formation in the three-disk system. The figure shows the three-disk system with its length scale double that of previous figures, with radius of hard magnets, distance between hard magnetic centers, radius of the soft-magnetic circle, and thickness of the sample taking the values 40, 150, 300, and 20 nm, respectively. The length scale L has to be compared with that of Fig. 1. Domain-wall formation becomes energetically favorable and frustration in the system is neutralized by domains which shield the influence of one hard disk on soft magnet from that of another.

HARD-SOFT MAGNETIC SYSTEM AS A TERNARY LOGIC DEVICE

The above discussion elucidates the fact that simple geometrical frustration results in rich magnetization patterns which vary according to the magnitude of the applied field. In all the four regimes mentioned above, the magnitude of the applied field was fixed at that of a particular regime and the field rotated to create the corresponding magnetization pattern and the system behavior. It is possible to use the system as a ternary logic device, whose logic states can be manipulated by controlling both the magnitude and the angle of the applied field. In the first regime, the system resides in one of the three equivalent minimum-energy states (see Fig. 1), and it can be thought of as being locked in one of the three available logic states and can be read out, without changing it. Since the first regime also includes zero applied field magnitude, the logic state of the system is preserved even without any external field and the memory is nonvolatile. To write, we increase the field to that of the third regime, rotate the field to switch the domain-wall shield to cover another pair of hard magnetic disks, and reduce the field to that of the first regime. This changes the logic state of the system predictably. Thus we can read and write the logic states of the system by manipulating the external magnetic field.

The writing scheme is depicted in Fig. 5. The figure shows the three phases of the writing operation. In the first phase, denoted by points between A and B in Fig. 5, the external field strength is gradually increased from 0 to 1000 Oe and the system stays close to the initial configuration, with the angle of average magnetization staying close to its initial value. This can be seen from section AB of the plot of average magnetization angle versus field strength. Energetically, the system now corresponds to the leftmost point of Fig. 2(c). In the second phase of operation, denoted by section BD, the external field strength is held constant and the angle is rotated by about 2.5 radians, until the first transition, as seen in Fig. 2(c), corresponding to the system jumping

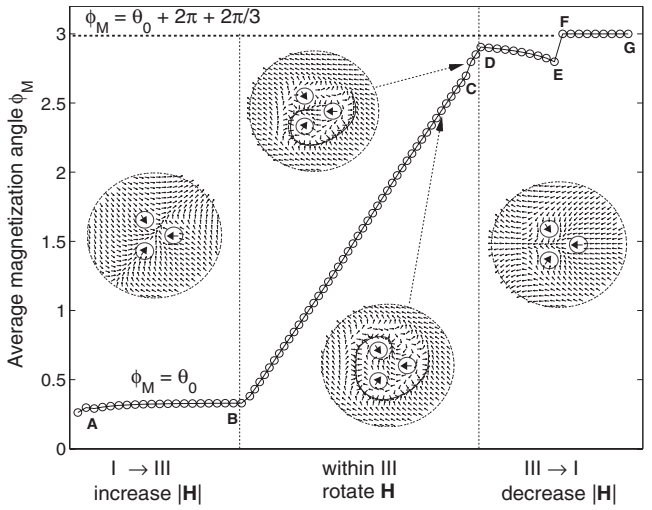

FIG. 5. An illustration of the three successive operations needed to change the logic state of the system. In the first phase, denoted by section AB of the figure, the system is taken from first to third regime by fixing the field direction at $\frac{\pi}{3}$ radians and increasing the magnitude from 0 to 1000 Oe. The average magnetization angle in the first phase is denoted as θ_0. The initial state of the system is shown as an inset in the leftmost part of the figure. In the second phase, denoted by section BD, the system is in the third regime, and the magnetic field is rotated through $2\pi+\frac{2\pi}{3}$. The logic state of the system changes as shown in the inset, with hardly noticeable change in the average magnetization near point C. The rightmost part shows the third phase, denoted by section DG, in which the magnetic-field magnitude is reduced from 1000 to 0 Oe, with its direction fixed. The abrupt transition from the third to first regime can be seen in the average magnetization plot, denoted by section EF. The average magnetization angle in the third phase is $\theta_0+2\pi+\frac{2\pi}{3}$. The system's changed logic state is shown as an inset of the rightmost part.

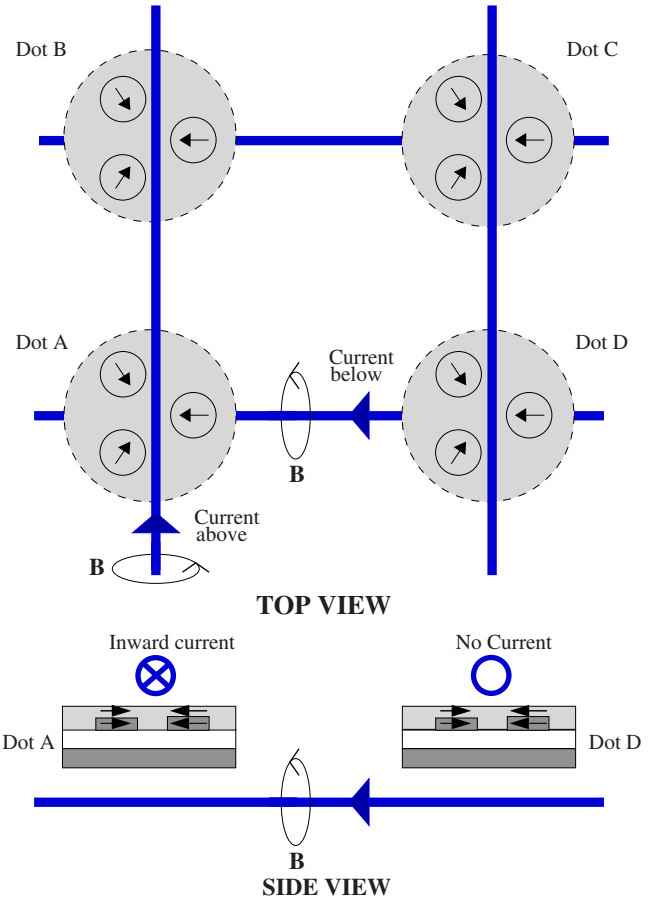

FIG. 6. (Color online) Schematic of a magnetic random access memory using the three-disk system. The dots are the magnetic tunnel junctions with the top soft-magnetic layer replaced by the three-disk system. Appropriately designed current pulses sent through horizontal and vertical wires create a rotating magnetic field at the position of dot A, changing its logic state. Judicious choice of geometrical parameters of the memory device and the absence of x, y, or both components of the write field at neighboring dots B, C, and D would lead to a field strength below the transition field to the third regime at these dots, thereby leaving their logic states unchanged. The side view shows the modified magnetic tunnel junction. The middle and the lower sections are the tunnel barrier and the fixed ferromagnetic layer, respectively. The magnetization direction of the fixed ferromagnetic layer is chosen such that the resistance of the tunnel junction is different for the three different logic states of the system. Leads for reading logic states are not shown.

from one metastable state to another, happens. The magnetization now switches from escaping through one neck, the region between two hard magnetic disks, to another. The signature of this transition on the average magnetization angle is weak and is barely visible near C in the plot of Fig. 5. In the third phase, denoted by section DG, the external field strength is reduced from 1000 to 0 Oe again. The system makes an abrupt transition from its metastable state to the closest of the three energy minima of the first regime. Section EF of the plot in Fig. 5 corresponds to the transition. Thus the logic state of the system is changed predictably by controlling the magnitude and direction of the external magnetic field.

This system can be incorporated into magnetic random access memory by replacing the free ferromagnetic layer of the magnetic tunnel junction with the system under consideration. Current pulses through a single horizontal and a vertical wire choose a specific dot (dot A in Fig. 6) to write a logic state. The pulses are designed such that they create the magnetic-field behavior in time and strength as required by the writing scheme mentioned above at the location of dot A, for instance. The neighbors of dot A would be unaffected as the magnetic-field strength at their locations is less than the critical field of transition into the third regime because of the lack of the x, y, or both components of the current-generated magnetic field at dots B, C, and D. The fixed ferromagnetic layer's magnetization direction is aligned such that the components of the magnetization of the three states of the system along the direction of the fixed layer's magnetization are unequal in magnitude. This condition ensures that the resistance of the magnetic tunnel junction is different for the three different logic states of the system, thus ensuring a reliable reading mechanism.

This ternary system would find use in applications where an additional logic state is needed to denote ambiguity, irrelevant information, and lack of data or error. The applications include hardwired embedded systems for queries which need real-time response, fault-tolerant circuits, digital logic design, expert systems, tristate cellular automata, etc. The advantage of this system over other existing ternary logic systems comes from the fact that this storage system is similar to the binary logic storage device using magnetic tunnel junctions and can be mass produced using the same tools.

CONCLUSIONS

We have investigated a soft-hard magnetic system with an interesting planar geometry and its transitions between frustrated local energy minima. Interplay between exchange, magnetostatic, and Zeeman interactions and the geometrical constraint imposed by hard magnets results in the display of complex magnetic patterns. We have identified four regimes of system behavior, parametrized by the external field magnitude, where the system exhibits different hysteretic properties, depending upon the dominant interactions in those regimes. This analysis illustrates the use of frustration in bringing out the rich physics resulting from competition between various interactions in the system. We have also pointed to an application of the system as a ternary logic device and outlined the operating mechanism of the device.

ACKNOWLEDGMENTS

We thank Hao Zeng for helpful discussions. This work has been supported by National Science Foundation under Grant No. DMR-0426826.

[1] Y. Qi, T. Brintlinger, and J. Cumings, Phys. Rev. B **77**, 094418 (2008).
[2] R. F. Wang, C. Nisoli, R. S. Freitas, J. Li, W. McConville, B. J. Cooley, M. S. Lund, N. Samarth, C. Leighton, V. H. Crespi, and P. Schiffer, Nature (London) **439**, 303 (2006).
[3] E. F. Kneller and R. Hawig, IEEE Trans. Magn. **27**, 3588 (1991).
[4] R. Coehoom, D. B. de Mooji, J. P. B. Duchateau, and K. H. J. Buschow, J. Phys. Colloq. **49**, C8 (1988).
[5] H. Zeng, J. Li, J. P. Liu, Z. L. Wang, and S. Sun, Nature (London) **420**, 395 (2002).
[6] E. E. Fullerton, J. S. Jiang, M. Grimsditch, C. H. Sowers, and S. D. Bader, Phys. Rev. B **58**, 12193 (1998).
[7] Eiichi Goto, Nobuo Hayashi, Takaaki Miyashita, and Keisuke Nakagawa, J. Appl. Phys. **36**, 2951 (1965).
[8] R. F. Sabiryanov and S. S. Jaswal, Phys. Rev. B **58**, 12071 (1998).
[9] R. F. Sabiryanov and S. S. Jaswal, J. Magn. Magn. Mater. **177-181**, 989 (1998).
[10] Giovanni Asti, Massimo Solzi, Massimo Ghidini, and Franco M. Neri, Phys. Rev. B **69**, 174401 (2004).
[11] J. E. Han and Vincent H. Crespi, Phys. Rev. Lett. **89**, 197203 (2002).
[12] H. C. Siegmann, J. Phys.: Condens. Matter **4**, 8395 (1992).
[13] R. Rohlsberger, H. Thomas, K. Schlage, E. Burkel, O. Leupold, and R. Ruffer, Phys. Rev. Lett. **89**, 237201 (2002).
[14] O. Hellwig, J. B. Kortright, K. Takano, and E. E. Fullerton, Phys. Rev. B **62**, 11694 (2000).
[15] C. Stamm, F. Marty, A. Vaterlaus, V. Weich, S. Egger, U. Maier, U. Ramsperger, H. Fuhrmann, and D. Pescia, Science **282**, 449 (1998).
[16] J. P. Hayes, IEEE Trans. Comput.-Aided Des. **CAD-5**, 274 (1976).
[17] K. C. Smith, IEEE Trans. Comput. **c-30**, 619 (1981).
[18] M. Mukaidono, IEEE Trans. Comput. **c-35**, 179 (1986).
[19] R. P. Cowburn, D. K. Koltsov, A. O. Adeyeye, M. E. Welland, and D. M. Tricker, Phys. Rev. Lett. **83**, 1042 (1999).
[20] Katsuyuki Naito, Hiroyuki Hieda, Masatoshi Sakurai, Yoshiyuki Kamata, and Koji Asakawa, IEEE Trans. Magn. **38**, 1949 (2002).
[21] C. J. Jiang and V. V. Tsukruk, Adv. Mater. (Weinheim, Ger.) **18**, 829 (2006).
[22] H. P. Oepen and J. Kirschner, Curr. Opin. Solid State Mater. Sci. **4**, 217 (1999).
[23] P. Moriarty, Rep. Prog. Phys. **64**, 297 (2001).
[24] S. D. Bader, Rev. Mod. Phys. **78**, 1 (2006).
[25] Stephen Y. Chou, Peter R. Krauss, and Linshu Kong, J. Appl. Phys. **79**, 6101 (1996).
[26] C. A. Ross, S. Haratani, F. J. Castano, Y. Hao, M. Hwang, M. Shima, J. Y. Cheng, B. Vogeli, M. Farhoud, M. Walsh, and Henry I. Smith, J. Appl. Phys. **91**, 6848 (2002).
[27] Charles Kittel, Rev. Mod. Phys. **21**, 541 (1949).
[28] M. C. Payne, M. P. Teter, D. C. Allan, T. A. Arias, and J. D. Joannopoulos, Rev. Mod. Phys. **64**, 1045 (1992).
[29] W. H. Press, S. A. Teukolsky, W. T. Vetterling, and B. P. Flannery, *Numerical Recipes in C* (Cambridge University Press, Cambridge, England, 1992).
[30] Andrew J. Newell, Wyn Williams, and David J. Dunlop, J. Geophys. Res. **98**, 9551 (1993).
[31] M. J. Donahue and D. G. Porter, OOMMF Version 1.1b2; http://math.nist.gov/oommf